Design of a High-Q Diamond-Loaded Cavity for a Third-Harmonic Subterahertz Gyrotron Driven by a Low-Power Electron Beam

Vitalii I. Shcherbinin, *Senior Member, IEEE*, Konstantinos A. Avramidis, Manfred Thumm, *Life Fellow, IEEE*, and John Jelonnek, *Senior Member, IEEE*

***Abstract*—A continuous-wave (CW) high-harmonic gyrotron driven by a low-power electron beam is a compact radiation source demanded by terahertz applications. Its physical feasibility, however, is hampered by ohmic losses and mode competition in the gyrotron cavity. An ultra-low-loss diamond loading of the cavity can give a clue to this problem. This article is concerned with theoretical aspects of mode selection and design for a gyrotron cavity loaded with coaxial rod made of chemical vapor deposition (CVD) diamond. As an example, the design of a high-Q diamond-loaded cavity for a third-harmonic 658-GHz gyrotron powered by a 0.1 A, 15 kV electron beam is presented. It is shown that the designed cavity enables the gyrotron to produce up to 116 W output power in a single oscillating mode.**

***Index Terms*— Gyrotrons, cyclotron harmonics, metal cavity, CVD diamond, ohmic losses, starting current**

I. Introduction

GROWING interest in dynamic nuclear polarization (DNP) enhanced nuclear magnetic resonance (NMR) spectroscopy generates the need for high-power and compact CW radiation sources operated in the sub-terahertz to terahertz frequency band [1]. In this frequency range, the most powerful oscillator is the gyrotron capable of producing from watts to kilowatts of output power. There are two design specifications, which are intended to make the gyrotron compact. The first specification is a high harmonic number s of the operating TE cavity mode, for which the required strength of the external magnetic field B_0 can be lowered by a factor of s. This makes it possible to reduce the size of the gyrotron magnetic system. The second specification is low power of the applied electron beam. It offers a means of reducing the size of an electron gun, power supply, collector, cooling and vacuum-pumping systems. In practice, the two specifications mentioned above are in conflict [2].

The reason is that the way to lower the electron beam power $P_b = I_b V_b$ is to reduce either or both the beam voltage V_b and current I_b. At the same time, because of diffractive and ohmic losses in the gyrotron cavity, the operating beam current I_b has a lower limit I_{st}, which is known as an oscillation threshold (or starting current) and which is governed by the following law [2], [3]:

$$I_{st} \propto \frac{\Gamma_s}{L^2 C_{ms} Q_{tot}}, \tag{1}$$

where $\Gamma_s = \gamma_0 \beta_{z0}^3 / \beta_{\perp 0}^{2s}$ [2], $\beta_{\perp 0} = \alpha \beta_{z0} = v_{\perp 0}/c$, $\beta_{z0} = v_{z0}/c$, c is the speed of light in vacuum, γ_0, α, $v_{\perp 0}$, and v_{z0} are the initial relativistic factor, pitch factor, transverse and axial velocities of beam electrons, respectively, L is the cavity interaction length, C_{ms} is the coefficient of beam coupling with the sth harmonic $\mathrm{TE}_{m,p}$ mode, $Q_{tot} = Q_{dif} Q_{ohm} / \left(Q_{dif} + Q_{ohm} \right)$, Q_{dif}, and Q_{ohm} are the total, diffractive, and ohmic quality factors of the $\mathrm{TE}_{m,p}$ mode, respectively. In a conventional-cavity gyrotron, $\mathrm{TE}_{m,p}$ mode is the eigenmode of an open-ended hollow cylindrical resonator with metal wall.

For fundamental ($s = 1$) modes excited by a weakly-relativistic electron beam, the relativistic parameter $\Gamma_1 = \gamma_0 \beta_{z0} / \alpha^2$ is much smaller than unity and vanishes, together with the oscillation threshold (1), as the beam voltage V_b approaches zero. That is why these modes have favorable oscillation conditions in a low-P_b regime, provided that there is no drastic degradation of the electron beam pitch factor α with decreasing V_b. This was demonstrated in a number of experimental studies [4]-[6].

In contrast, for high-harmonic ($s \geq 2$) modes, the relativistic parameter Γ_s is large and tends to infinity as $V_b \to 0$. For $V_b = 15$ kV and $\alpha = 1.2$, as an example, $\Gamma_1 = 0.11$, $\Gamma_2 = (5.5)^2 \Gamma_1$, $\Gamma_3 = (5.5)^4 \Gamma_1$. In this case, the starting current of the $\mathrm{TE}_{m,p}$ mode excited at the second or

Manuscript received X.X.XXXX.

The work of V. I. Shcherbinin was supported by the Georg Forster Research Fellowship for Experienced Researchers from the Alexander von Humboldt Foundation.

V. I. Shcherbinin is with the Institute for Pulsed Power and Microwave Technology (IHM), Karlsruhe Institute of Technology (KIT), 76131 Karlsruhe, Germany, and also with the National Science Center "Kharkiv Institute of Physics and Technology", 61108 Kharkiv, Ukraine (e-mail: vshch@ukr.net).

K. A. Avramidis, M. Thumm and J. Jelonnek are with the Institute for Pulsed Power and Microwave Technology (IHM), Karlsruhe Institute of Technology (KIT), 76131 Karlsruhe, Germany.

third cyclotron harmonic is more than 30 or 900 times as high as that of fundamental $TE_{m,p}$ mode, provided that C_{ms} is kept fixed.

According to (1), the most efficient way to reduce the starting currents of high-harmonic modes is to increase the interaction length L of the gyrotron cavity. The increase of L is accompanied by reduced diffractive losses of the cavity. On the one hand, this effect is beneficial, since it enhances the total quality factor Q_{tot} and thus initiates further decrease of the oscillation threshold (1). However, on the other hand, it lowers the gyrotron efficiency by a factor of $\left(1+Q_{dif}/Q_{ohm}\right)$. In a conventional gyrotron cavity, Q_{dif} scales as cube of L [7], while Q_{ohm} has an upper limit equal to the ratio of the wall radius R to the skin depth δ_s [8]. This gives an insight into why cavity ohmic losses often constitute more than 80% of the power of DNP gyrotrons operated at the second ($s=2$) cyclotron harmonic [9]-[12]. Since the ohmic losses also reduce the beam-wave interaction efficiency [13], the net (output) efficiency of low-P_b second-harmonic gyrotrons can be as low as 1% [10], [11], [14]-[16]. In view of these facts, a compact third-harmonic ($s=3$) gyrotron driven by a low-power electron beam seems hardly feasible, even in theory. This is in contrast to high-harmonic gyro-devices with electron beam power equal to hundreds of kilowatts [17]-[22].

Moreover, as discussed above, low-harmonic competing modes naturally have much lower oscillation thresholds than that of the operating mode of a low-voltage high-harmonic gyrotron. In such situation, mode competition is a problem of great concern and much care must be taken in mode selection [23]-[27], especially when $s \geq 3$ [28]-[31]. This makes the design of a third-harmonic gyrotron driven by a low-power electron beam even more challenging.

An alternative way to reduce the oscillation threshold of a high-harmonic gyrotron is to load the gyrotron cavity with a coaxial rod made of ultra-low-loss diamond [32]. Such a diamond-loaded cavity is capable of supporting TE modes with high ohmic Q-values. Because of this, the total quality factor Q_{tot} and the ratio of diffractive-to-ohmic losses of the diamond-loaded cavity can far exceed those of a conventional cavity having the same Q_{dif}. As a consequence, increase of the length L of the diamond-loaded cavity provides a means for marked decrease of the oscillation threshold (1) without drastic degradation of gyrotron efficiency. In addition, the beam-wave coupling coefficients C_{ms} of high-Q modes can be larger than those of TE modes supported by a conventional gyrotron cavity [32]. Taken together, the above-listed advantages of high-Q diamond-loaded cavities can make them particularly suitable for use in low-P_b high-harmonic gyrotrons demanded by DNP-NMR spectroscopy.

However, there are a number of fundamental problems and technical challenges that still remain to be addressed before the diamond-loaded cavities could be put to practical use. Among emerging technical challenges are high-precision manufacturing, robust holding and strict alignment of the diamond rod, heat removal from the diamond rod, and prevention of charging of the diamond rod. At the moment, it is an open question whether or not the currently available technologies are capable of meeting these challenges. This question goes beyond the scope of our present theoretical study.

The crucial fundamental problem is the mode competition, which was not considered in [32]. This problem alone can negate all potential advantages provided by diamond-loaded cavities for low-voltage high-harmonic gyrotrons. Compared to conventional cavities, these cavities have a much richer spectrum of normal modes. Therefore, a new strategy is required to select the appropriate operating mode of a high-harmonic gyrotron equipped with diamond-loaded cavity. This article presents such a strategy, using a third-harmonic 658-GHz gyrotron powered by a 1.5 kW electron beam as an example.

II. Mode classification

First, we give an overview of basic properties of normal modes of a metal gyrotron cavity loaded with a coaxial dielectric rod [32], [33]. The metal cavity has the wall radius R and conductivity σ. The radius and relative complex permittivity of the dielectric rod are R_i and $\varepsilon=\varepsilon_r\left(1+i\tan\delta\right)$, respectively. In the general case, the normal modes of the dielectric-loaded cavity are hybrid modes [34], [35]. The exceptions are cutoff TE and TM modes.

TE modes excited near cutoff frequencies are of prime interest for gyrotrons. In the transverse cross-section of the gyrotron cavity with coaxial dielectric rod, these modes have the following field structure [33]:

$$H_z = k_\perp^2 \Psi\left(k_\perp r\right)\exp\left(-i\omega t+im\varphi\right) \qquad (2)$$
$$E_\varphi = -ikk_\perp \Psi'\left(k_\perp r\right)\exp\left(-i\omega t+im\varphi\right)$$

where $k_\perp$ is the transverse wavenumber and $\Psi\left(k_\perp r\right)$ is the membrane function. In the vacuum region ($R_i<r<R$), $k_\perp = k = \omega/c$ and $\Psi\left(k_\perp r\right) = J_m\left(k_\perp r\right) - AN_m\left(k_\perp r\right)$, where $J_m(\cdot)$ and $N_m(\cdot)$ are the m-th order Bessel and Neumann functions, respectively. In the dielectric region, $k_\perp=\sqrt{\varepsilon}k$ and $\Psi\left(k_\perp r\right) = BJ_m\left(k_\perp r\right)$.

The unknown constants A and B are related by the impedance-like boundary conditions at the surfaces $r=R$ and $r=R_i$ [33], [35]. From these conditions, one obtains

$$A = \frac{J_m'(x) - iZ_s J_m(x)}{N_m'(x) - iZ_s N_m(x)} = \frac{D_v(x)}{\nu_v(x)} \qquad (3)$$

$$A = \frac{J_m'\left(\sqrt{\varepsilon}y\right)J_m(y) - \sqrt{\varepsilon}J_m\left(\sqrt{\varepsilon}y\right)J_m'(y)}{J_m'\left(\sqrt{\varepsilon}y\right)N_m(y) - \sqrt{\varepsilon}J_m\left(\sqrt{\varepsilon}y\right)N_m'(y)} = \frac{\nu_d(y)}{D_d(y)} \qquad (4)$$

where $x=kR$, $y=kR_i$, $Z_s=(1-i)k\delta_s/2$ is the normalized surface impedance of the cavity wall, and $\delta_s=\sqrt{2/(\mu_0\omega\sigma)}$ is the skin-depth.

The dispersion relation $D(\omega)=0$ can be found by equating (3) and (4). This yields

$$D(\omega)=D_v(x)D_d(y)+\nu(\omega)=0 \qquad (5)$$

where $\nu(\omega)=-\nu_v(x)\nu_d(y)$. Solutions of the dispersion relation (5) are the complex cutoff frequencies $\omega=2\pi f_c\left(1-i/(2Q_{ohm})\right)$ of TE modes of a metal cylindrical cavity loaded with a coaxial dielectric rod. Fig. 1 shows these solutions for low-order $TE_{11,p}$ modes ($p=1,2,3...$).

We will try to classify these solutions. In the extreme case $\nu(\omega)=0$, the dispersion relation (5) reduces to equations $D_v(x)=0$ and $D_d(y)=0$, which have independent solutions $x=x_{m,n}$ and $y=y_{m,n}$ ($n=1,2,3...$) and describe two uncoupled types of TE modes. These idealized modes will be called the vacuum (V) and dielectric (D) modes. The cutoff frequencies of $V_{m,n}$ modes are found from the equations $x=x_{m,n}$ and depend only on the radius and conductivity of the cylindrical metal cavity (Fig. 1a). In contrast, the $D_{m,n}$ modes satisfy the equations $y=y_{m,n}$ and are determined only by the radius and permittivity of the dielectric rod (Fig. 1b). Obviously, ohmic losses of V and D modes are independent of the material properties of dielectric rod and cavity wall, respectively.

In actual fact, the coupling of V and D modes is nonzero and depends on the function $\nu(\omega)$. It is weak, provided that the condition $|\nu|<<|D_vD_d|$ holds true. Under this condition, the normal TE modes of a cylindrical metal cavity loaded with a coaxial dielectric rod can be classified as vacuum-like (VL) and dielectric-like (DL) modes. The eigenvalues of VL and DL $TE_{m,p}$ modes are close to $x=x_{m,n}$ and $y=y_{m,n}$ ($n\neq p$), respectively. Strong coupling of these modes is observed in the vicinities of simultaneous solutions of equations $D_v(x)=0$ and $D_d(y)=0$. In these frequency regions, the cutoff frequencies of VL and DL modes undergo the anti-crossing phenomenon (Fig. 1).

As can be seen from Fig. 1, a cylindrical metal cavity loaded with a coaxial dielectric rod can only support a few DL modes, which have the eigenvalues close to the first few solutions $y=y_{m,n}$ of the equation $D_d(y)=0$. These modes have high ohmic Q-values in a gyrotron cavity loaded with an ultra-low-loss dielectric rod. In Fig. 1, the material parameters of such a rod correspond to the chemical vapor deposition (CVD) diamond with $\varepsilon_r=5.7$ and $\tan\delta=10^{-5}$ [36]-[38].

Vacuum-like and dielectric-like $TE_{m,p}$ modes differ in coupling with a helical electron beam in the dielectric-loaded cavity. In this cavity, the coefficient of beam-wave coupling has the following form [33], [39]:

$$C_{ms}=\left[J_{m-s}(k_\perp r_b)-AN_{m-s}(k_\perp r_b)\right]^2/P_{mp} \qquad (6)$$

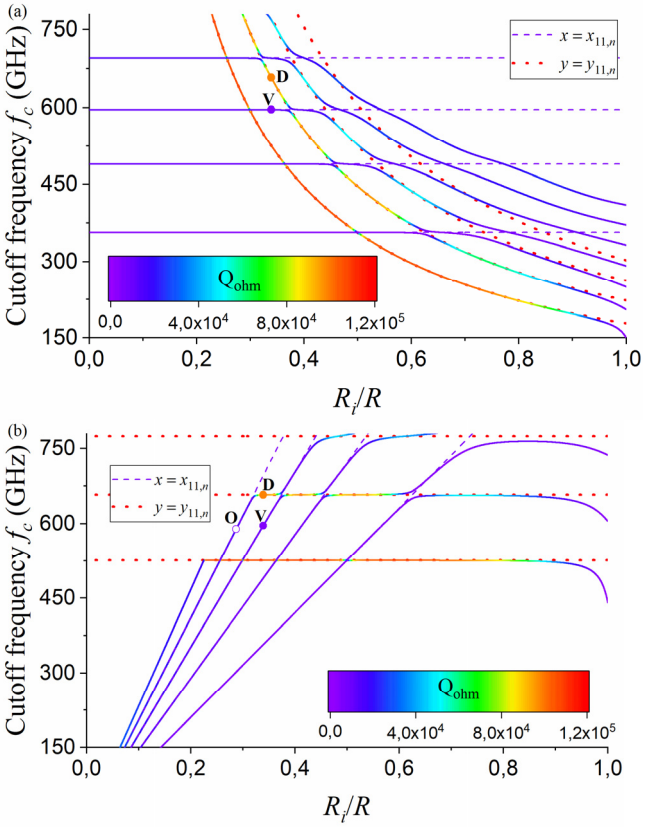

Fig. 1. Cutoff frequencies and ohmic Q-values of normal $TE_{11,p}$ modes of the cylindrical metal cavity loaded with a coaxial diamond rod versus the radius ratio R_i/R for (a) R = 1.715 mm and (b) R_i = 0.581 mm ($\sigma=2.9\times10^7$ S/m, $\varepsilon_r=5.7$, $\tan\delta=10^{-5}$)

where r_b is the beam radius, $P_{mp}=2\int_0^R rdr\left[k_\perp^2\Psi'^2+m^2r^{-2}\Psi^2\right]$ is the normalized power flow through the transverse cross-section of the dielectric-loaded cavity.

Fig. 2 shows the beam-wave coupling coefficients for the co-rotating ($m=11$) VL mode and for the counter-rotating ($m=-11$) DL mode, which are symbolized by **V** and **D** in Fig. 1, respectively. In essence, the fundamental difference of these coefficients is attributed to the field amplitude A (see (3) and (4)), which satisfies the conditions $|A|<<1$ and $|A|>>1$ for the VL and DL modes, respectively. As a consequence, compared to the VL modes, the DL modes have larger denominators P_{mp} in (6) and thus weaker coupling with the electron beam in the greater part of the interaction region (Fig. 2). Despite this fact, the coefficients C_{ms} for DL modes can exceed those for VL modes, if the beam radius r_b is positioned relatively close to the radius R_i of the dielectric loading. This requires the DL modes to be counter-rotating ($m<0$) modes. The reason is that the square of the Neumann function $N_{m-s}(k_\perp r_b)$ in the numerator of (6) grows rapidly with decreasing argument and increasing absolute value $|m-s|$ of the order. That is why the peak beam-wave coupling

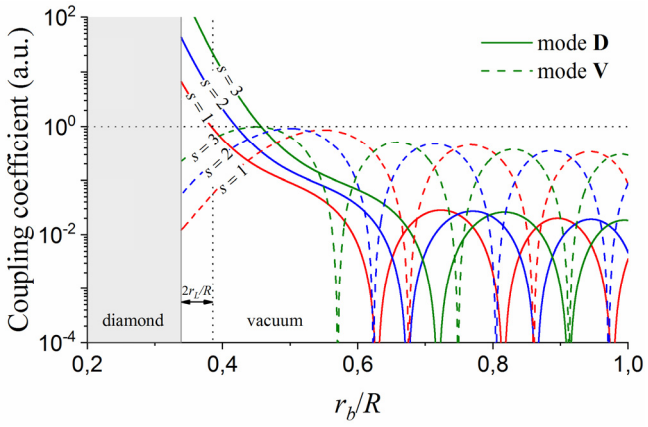

Fig. 2. Normalized coefficients C_{ms} of beam coupling with co-rotating (m = 11) mode **V** and counter-rotating (m = -11) mode **D** of the diamond-loaded cavity. Here the Larmor radius r_L of beam electrons is shown for B_0 = 8.05 T, V_b = 15 kV, and α = 1.2.

coefficient of the counter-rotating DL mode **D** is attained for $r_b = R_i$ and far exceeds that of the VL mode **V** (Fig. 2). Moreover, it grows rapidly with increasing number s of cyclotron harmonic. Note that this peak cannot be reached because of the finite beam thickness. The beam guiding-center radius r_b must be larger than $R_i + r_L$, even if an idealized beam with electron Larmor radius r_L is considered. In the following, we will use $R_i + 2r_L$ as the lower theoretical limit of r_b.

III. Mode Selection and Cavity Design

The ultimate objective is to design a diamond-loaded cavity for a third-harmonic gyrotron operated in a high-Q DL mode. As discussed above, for strong coupling of such a mode with the electron beam, the beam radius r_b must be positioned sufficiently close to the radius R_i of the diamond rod. It is reasonable to expect that, under this requirement, the most dangerous competitors in a third-harmonic gyrotron will be the first- and second-harmonic DL modes. Therefore, first and foremost, it is essential to select the operating DL mode, which is well separated from such competitors.

Fig. 3a shows cutoff frequencies $f_c = c\,\mathrm{Re}\left(y_{m,n}\right)/\left(2\pi R_i\right)$ of the first-, second- and third-harmonic $D_{m,n}$ modes for $R_i = 0.581$ mm. Among them are several promising candidates for the operating mode of a third-harmonic gyrotron. However, when deciding on the choice of the operating mode, it is important to keep in mind two facts. On the one hand, the lower is $n/|m|$ for a DL mode with the eigenvalue $y \approx y_{m,n}$, the higher is the ohmic Q-value (Fig. 1). On the other hand, the high-Q DL modes with ultra-low ratios $n/|m|$ feature weak coupling ($\nu(\omega) \approx 0$) with VL modes (see the lowest-order DL mode in Fig. 1). Such modes are nearly insensitive to the radius R of the cavity wall. Thus, wall profiling cannot be applied to optimize their field structure inside the diamond-loaded cavity. This property makes the DL

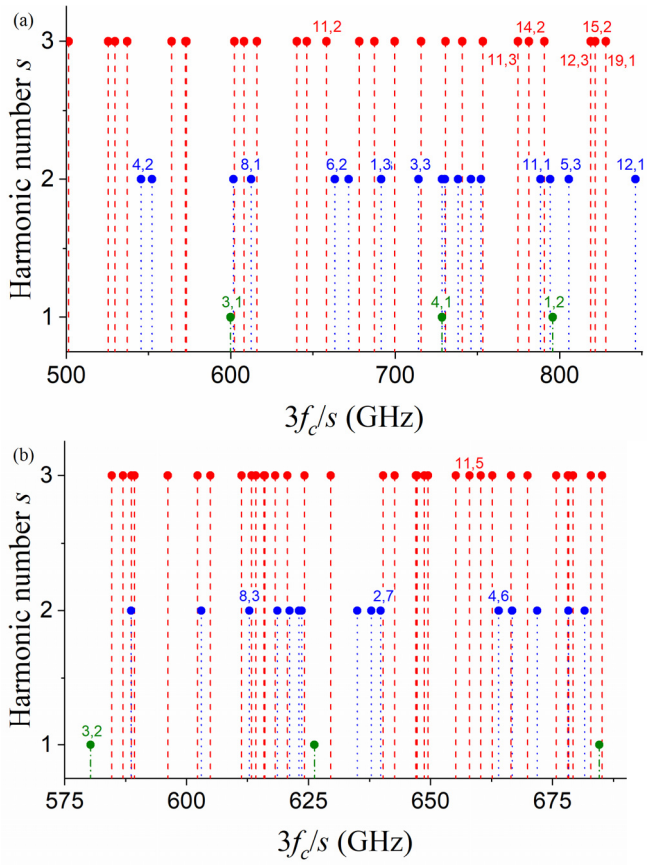

Fig. 3. (a) Cutoff frequencies of the sth harmonic modes for ε_r = 5.7, R_i = 0.581 mm, R = 1.715 mm: (a) idealized $D_{m,n}$ modes of the insert and (b) $TE_{m,p}$ modes of the diamond-loaded cavity.

modes with ultra-low ratios $n/|m|$ unattractive as operating modes. Using the above line of reasoning, we adopt the DL mode with the eigenvalue $y \approx y_{11,2}$ ($|m| = 11$, $n = 2$) as a good candidate for the operating third-harmonic mode. Here we do not distinguish between co- and counter-rotating modes, which are degenerate in a cold cavity.

With rare exception, the chosen candidate mode depends only slightly on the radius R of the cavity wall (see Fig. 1b). Therefore, the cavity radius can be adjusted to provide the maximal frequency separation of the operating DL mode from competing VL modes. In such procedure, the emphasis should be placed on low-harmonic backward-wave competitors, which usually present the main obstacle to operation of high-harmonic gyrotrons [23], [26], [27], [31], [33], [40]. By this means one obtains the radius $R = 1.715$ mm of the main section of the designed cavity. For this cavity section loaded with a uniform diamond rod of radius $R_i = 0.581$ mm, the cutoff frequencies of the operating and competing $TE_{m,p}$ modes are shown in Fig. 3b. The operating mode is the $TE_{11,5}$ mode ($|m| = 11$, $p = 5$), which corresponds to the fifth solution of the dispersion relation (5) and is symbolized by **D** in Fig. 1. The cutoff frequency and ohmic Q-value of this mode are 658 GHz and 95600, respectively.

In the case $|\nu| >> |D_v D_d|$, the operating DL mode features strong coupling with VL modes. This provides a means for

proper profiling of the metal cavity loaded with a uniform diamond rod. Such wall profiling serves to offer minimal leakage of the operating mode from the cavity input, small conversion of the operating mode to spurious modes and high-purity transformation of the operating DL mode to the outgoing VL $TE_{11,4}$ mode ($|m|=11$, $p=4$), which is symbolized by **O** in Fig. 1b. Fig. 4a shows the design of the profiled diamond-loaded cavity, which is jointed to a hollow output waveguide.

The coupled-mode approach of [32], [41] was used to calculate the amplitudes of the operating near-cutoff mode and spurious radial modes. For the length $L=19$ mm of the main cavity section, these amplitudes are shown in Fig. 4b. It should be stressed that the spurious far-from-cutoff modes are hybrid modes inside the diamond-loaded cavity, but are converted to vacuum TE and TM modes in the hollow output waveguide. As Fig. 4b suggests, the outgoing mode of the output waveguide is nearly a pure vacuum $TE_{11,4}$ mode. This V mode can be extracted from a gyrotron using a standard quasi-optical output coupler.

Because of small mode conversion inside the diamond-loaded cavity, the operating $TE_{11,5}$ mode can be well approximated by a single mode with varying cutoff frequency $f_c\left(R(z)\right)$ (see Fig. 1b). Results of such single-mode approximation (SMA), which is often called Vlasov approach [42], are depicted in Fig. 4b for comparison purpose. This suggests that the performance of a third-harmonic gyrotron with diamond-loaded cavity can be calculated by single-mode self-consistent equations known as gyrotron equations [13], [43].

IV. Gyrotron Performance

As a designed gyrotron we consider a third-harmonic 658-GHz gyrotron. The tube is equipped with a copper cavity loaded with a CVD diamond rod (Fig. 4a) and operates in the dielectric-like $TE_{11,5}$ mode. The cavity wall is assumed to have the DC conductivity $\sigma=2.9\times10^7$ S/m, which is equal to half of that of ideal OFHC copper. The parameters of the electron beam are as follows: beam current $I_b=0.1$ A, beam voltage $V_b=15$ kV, pitch factor $\alpha=1.2$. In simulations, the velocity spread $\delta v_\perp$ of the beam electrons is assumed to be zero, unless otherwise stated. In the following, we will use the notation $TE_{m,p}$ mode for one of the $TE_{+|m|,p}$ and $TE_{-|m|,p}$ modes, which has the largest beam-wave coupling coefficient (6).

First, the beam radius is set to $r_b=R_i+2r_L$ with r_L equal to 0.04 mm. For such beam radius, the cavity length L can be optimized to ensure the highest possible output efficiency. This gives the optimal cavity length $L=19$ mm, mentioned in Section III. This length is not optimal with respect to interaction efficiency because of ohmic losses in the cavity [2], [13]. For $L=19$ mm, the cold diffractive Q_d, ohmic

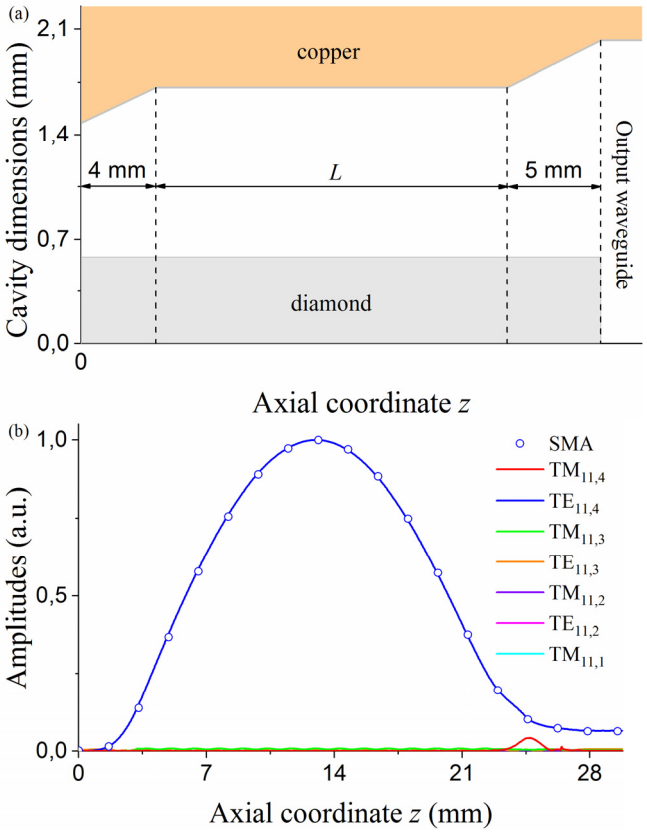

Fig. 4. (a) Structure of the diamond-loaded cavity and (b) amplitudes of the normal cavity modes for L = 19 mm, where the same mode nomenclature is used as that for normal TE and TM modes of the output waveguide.

Q_{ohm}, and total Q_{tot} quality factors of the operating mode are equal to 83000, 94400 and 44400, respectively.

Fig. 5a shows the starting currents of the operating and competing modes of the third-harmonic 658-GHz gyrotron equipped with the designed diamond-loaded cavity. It can be seen that the most dangerous competing modes are the first-harmonic $TE_{3,2}$ mode and second-harmonic $TE_{8,3}$ mode, which originate from the idealized $D_{3,1}$ and $D_{8,1}$ modes (see Fig. 3a), respectively. For the design parameters in hand, however, these competitors have sufficiently high starting currents and therefore pose no threat to the operating $TE_{11,5}$ mode, which is the only oscillating mode in the range of magnetic fields from 8.03 to 8.08 T. In this range, the peak output power of the third-harmonic 658-GHz gyrotron is 116 W for a beam velocity spread $\delta v_\perp=5$ % (Fig. 6a). This peak power corresponds to a gyrotron efficiency of 7.7 %. By comparison, in [2], an efficiency of 1.6% was theoretically predicted for a conventional-cavity third-harmonic 0.4-THz gyrotron driven by an electron beam having the same voltage $V_b=15$ kV and pitch factor $\alpha=1.2$, but much higher beam current $I_b=3$ A.

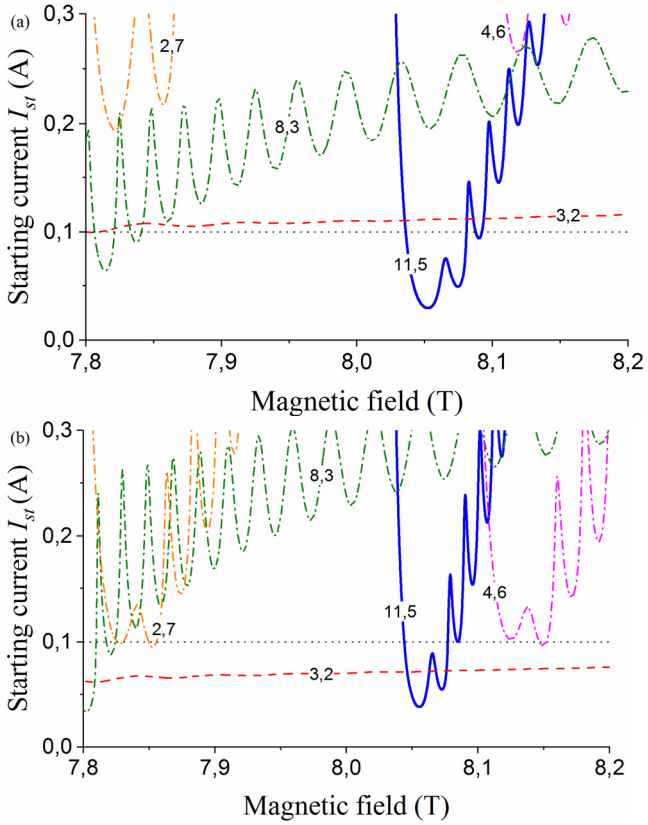

Fig. 5. Starting currents of the operating $TE_{11,5}$ mode and competing $TE_{m,p}$ modes of the third-harmonic 658-GHz gyrotron equipped with diamond-loaded cavity for (a) $r_b = R_i + 2r_L$, $L = 19$ mm and (b) $r_b = R_i + 3r_L$, $L = 25$ mm. The velocity spread is assumed to be zero.

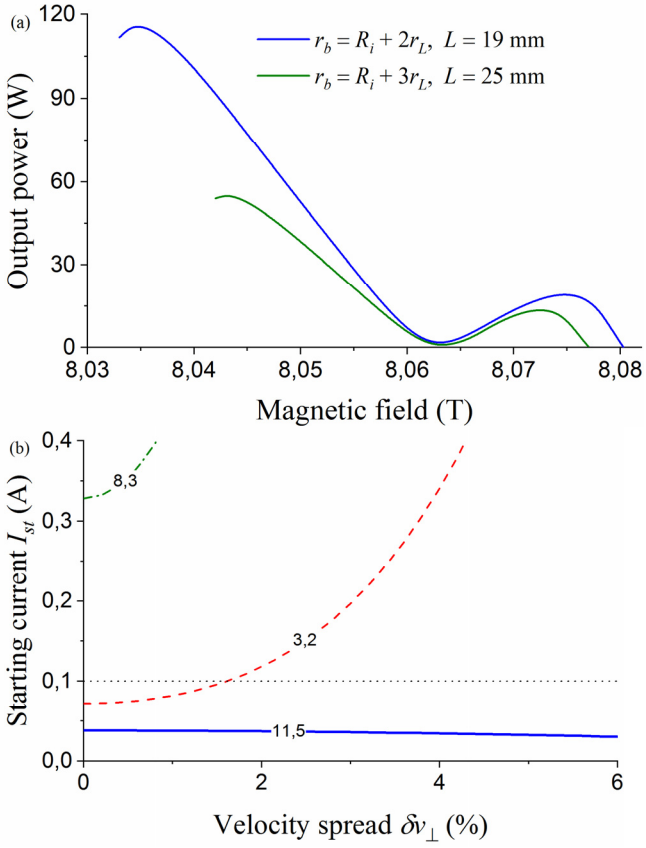

Fig. 6. (a) Output power of the third-harmonic 658-GHz gyrotron driven by a 0.1 A, 15 kV electron beam for two designs of the diamond-loaded cavity ($\delta v_\perp = 5$ %) and (b) starting currents of the operating and competing modes versus the velocity spread $\delta v_\perp$ of beam electrons for $B_0 = 8.055$ T, $r_b = R_i + 3r_L$, $L = 25$ mm.

In view of finite beam thickness, which is typically smaller than a quarter of the operating wavelength [44], it is desirable to keep the beam radius r_b as far away from the diamond rod as possible. Therefore we next increase r_b from $r_b = R_i + 2r_L$ to $r_b = R_i + 3r_L$. This involves a decrease of the beam-wave coupling coefficient C_{ms} for the operating DL mode (Fig. 2). To compensate for the decrease of C_{ms}, the optimal cavity length L was increased to 25 mm. For this length, the cold diffractive Q_d, ohmic Q_{ohm}, and total Q_{tot} quality factors of the diamond-loaded cavity are 176000, 95000 and 61700, respectively

For the modified design parameters of the third-harmonic 658-GHz gyrotron, the starting currents of the operating and competing modes are shown in Fig. 5b. It can be seen that, in general, increase of the beam radius has an unfavorable effect on the excitation of the operating $TE_{11,5}$ mode. The reason is that, the operating DL mode features a beam-wave coupling coefficient (Fig. 2), which tends to decrease more rapidly with increasing beam radius than those of competing modes. As a result, increase of the beam radius enlarges the number of probable competing modes supported by the diamond-loaded cavity. Among them the most dangerous is the first-harmonic $TE_{3,2}$ mode, which has now a starting current of about 0.07 A and therefore may hinder the operation of the third-harmonic 658-GHz gyrotron. Unlike the operating $TE_{11,5}$ mode, this mode is a backward-wave mode with high axial index. Therefore, in actual conditions, it is subject to strong suppression by an electron beam with nonzero velocity spread [31]. This is evident from Fig. 6b. It is seen that the competing $TE_{3,2}$ mode is well suppressed by the electron beam, even for a low velocity spread $\delta v_\perp \le 3$ %. Such situation is favorable for the near-cutoff operating $TE_{11,5}$ mode, which is only slightly affected by low $\delta v_\perp$. As a result, for $\delta v_\perp = 5$ %, this mode is free from any competing modes (Fig. 6b) and can attain 55 W of the peak output power with an efficiency of 3.7 % (Fig. 6a).

V. Conclusions

It has been shown that near-cutoff TE modes of a metal gyrotron cavity loaded with a coaxial dielectric rod can be classified as coupled vacuum-like (VL) and dielectric-like (DL) modes. The VL modes have much in common with vacuum (V) TE modes of a hollow metal cavity. Unlike the VL modes, the DL modes are generally little sensitive to radius and material of the cavity wall, since their fields are mostly concentrated inside the dielectric rod. For this reason, the DL modes feature high ohmic Q-values in a metal cavity with dielectric rod made of ultra-low-loss material, such as CVD diamond. The beam-wave coupling coefficients of these modes exceed those of the VL modes, provided that the beam is positioned relatively close to the dielectric rod. More

important, the beam coupling coefficients of DL modes increase with the number of cyclotron harmonic. An appropriate candidate for the operating mode of a third-harmonic 658-GHz gyrotron has been selected among the high-Q DL modes of a diamond-loaded cavity. For this mode, the cavity design has been optimized to rarefy the spectrum of competing modes and to provide high-purity transformation of the operating DL mode to an outgoing V mode of the hollow output waveguide. The cavity length has been adjusted to maximize the output power of the third-harmonic 658-GHz gyrotron powered by 0.1 A, 15 kV electron beam. It has been shown that this gyrotron is free from competing modes and capable of producing up to 116 W output power with an efficiency of 7.7 % for 5 % velocity spread of the beam electrons. The obtained efficiency is above the highest efficiency 2.8% achieved by existing second-harmonic DNP gyrotrons at $f = 526$ GHz, with $I_b = 0.6$ A and $V_b = 15$ kV [12]. Such a benefit of a diamond-loaded cavity could compensate for complexity of its use in compact high-harmonic terahertz gyrotrons demanded by DNP-NMR spectroscopy and thus provides impetus to further investigation of the proposed concept.

REFERENCES

[1] R. G. Griffin, T. M. Swager, and R. J. Temkin, "High frequency dynamic nuclear polarization: New directions for the 21st century," *J Magn. Reson.*, vol. 306, p. 128-133, Sep. 2019, doi: 10.1016/j.jmr.2019.07.019.

[2] M. Y. Glyavin, N. A. Zavolskiy, A. S. Sedov, and G. S. Nusinovich, "Low-voltage gyrotrons," *Phys. Plasmas*, vol. 20, no. 3, p. 033103, Mar. 2013, doi: 10.1063/1.4791663

[3] B. G. Danly, and R. J. Temkin, "Generalized nonlinear harmonic gyrotron theory," *Phys. Fluids*, vol. 29, no. 2, pp. 561–567, Feb. 1986, doi: 10.1063/1.865446.

[4] M. K. Hornstein, V. S. Bajaj, R. G. Griffin, and R. J. Temkin, "Efficient low-voltage operation of a CW gyrotron oscillator at 233 GHz," *IEEE Trans. Plasma Sci.*, vol. 35, no. 1, pp. 27–30, Feb. 2007, doi: 10.1109/TPS.2006.889295

[5] V. L. Bratman, A. E. Fedotov, A. P. Fokin, M. Yu. Glyavin, V. N. Manuilov, and I. V. Osharin, "Operation of a sub-terahertz CW gyrotron with an extremely low voltage," *Phys. Plasmas*, vol. 24, no. 7, p. 113105, doi: 10.1063/1.5000481

[6] A. Kuleshov, E. Khutoryan, S. Kishko, S. Ponomarenko, M. Glyavin, I. Bandurkin, V. Manuilov, A. Fedotov, T. Saito ,Y. Ishikawa, Y. Tatematsu, S. Mitsudo, and T. Idehara, "Low-voltage operation of the double-beam gyrotron at 400 GHz," *IEEE Trans. Electron Devices*, vol. 67, no. 2, pp. 673-676, Feb. 2020, doi: 10.1109/TED.2019.2957873.

[7] Y. J. Huang, L. H. Yeh, and K. R. Chu, "An analytical study on the diffraction quality factor of open cavities," *Phys. Plasmas*, vol. 21, no. 10, p. 103112, Oct. 2014, doi: 10.1063/1.4900415.

[8] S. N. Vlasov, L. I. Zagryadskaya, and M. I. Petelin, "Resonators and waveguides having "whispering gallery" modes for cyclotron-resonance masers," *Radiophys. Quantum Electron*., vol. 16, no. 11, Nov. 1973, pp. 1348–1353, doi: 10.1007/BF01080919.

[9] La Agusu, T. Idehara, H. Mori, T. Saito, I. Ogawa, and S. Mitsudo, "Design of a CW 1 THz gyrotron (Gyrotron FU CW III) using a 20 T superconducting magnet," *Int. J Infrared Millim. Waves*, vol. 25, no. 5, pp. 315–328, May 2007, doi: 10.1007/s10762-007-9215-y.

[10] A. C. Torrezan, S. T. Han, I. Mastovsky, M. A. Shapiro, J. R. Sirigiri, R. J. Temkin, A. B. Barnes, and R. G. Griffin, "Continuous-wave operation of a frequency-tunable 460-GHz second-harmonic gyrotron for enhanced nuclear magnetic resonance," *IEEE Trans. Plasma Sci.*, vol. 38, no. 6, pp. 1150–1159, Jun. 2010, doi: 10.1109/TPS.2010.2046617.

[11] S. K. Jawla, R. G. Griffin, I. A. Mastovsky, M. A. Shapiro and R. J. Temkin, "Second harmonic 527-GHz gyrotron for DNP-NMR: Design and experimental results," *IEEE Trans. Electron Devices*, vol. 67, no. 1, pp. 328–334, Jan. 2020, doi: 10.1109/TED.2019.2953658.

[12] M. Yu. Glyavin, A. N. Kuftin, M. V. Morozkin, M. D. Proyavin, A. P. Fokin, A. V. Chirkov, V. N. Manuilov, A. S. Sedov, E. A. Soluyanova, D. I. Sobolev, E. M. Tai, A. I. Tsvetkov, A. G. Luchinin, S. Yu. Kornishin, and G. G. Denisov, "A 250-Watts, 0.5-THz continuous-wave second-harmonic gyrotron," *IEEE Electron Device Letters*, 2021, doi: 10.1109/LED.2021.3113022.

[13] V. I. Shcherbinin, A. V. Hlushchenko, A. V. Maksimenko, and V. I. Tkachenko, "Effect of cavity ohmic losses on efficiency of low-power terahertz gyrotron," *IEEE Trans. Electron Devices*, vol. 64, no. 9, pp. 3898–3903, Sep. 2017, doi: 10.1109/TED.2017.2730252.

[14] M. K. Hornstein, V. S. Bajaj, R. G. Griffin, and R. J. Temkin, "Continuous-wave operation of a 460-GHz second harmonic gyrotron oscillator," *IEEE Trans. Plasma Sci.*, vol. 34, no. 3, pp. 524–533, Jun. 2006, doi: 10.1109/TPS.2006.875769.

[15] T. Idehara, I. Ogawa, L. Agusu, T. Kanemaki, S. Mitsudo, and T. Saito., "Development of 394.6 GHz CW gyrotron (gyrotron FU CW II) for DNP/proton-NMR at 600 MHz," *Int. J Infrared Millim. Waves*, vol. 28, no. 6, pp. 433–442, Jun. 2007, doi: 10.1007/s10762-007-9224-x.

[16] T. Idehara, K. Kosuga, L. Agusu, I. Ogawa, H. Takahashi, M. E. Smith, and R. Dupree, "Gyrotron FU CW VII for 300 MHz and 600 MHz DNP-NMR spectroscopy," *J. Infrared Millim. Terahertz Waves*, vol. 31, no. 7, pp. 763–774, Jul. 2010, 10.1007/s10762-010-9637-9.

[17] X.-B. Qi, C.-H. Du, J.-F. Zhu, S. Pan, and P.-K. Liu, "The design of a multi-harmonic step-tunable gyrotron," *Phys. Plasmas*, vol. 24, no. 3, p. 033101, Mar. 2017, doi: 10.1063/1.4977452.

[18] Y. S. Yeh, W. J. Kao, L. J. Li, and Y. W. Guo, "Comparative analysis of fourth-harmonic multiplying gyrotron traveling-wave amplifiers operating at different frequency multiplications," *Phys. Plasmas*, vol. 24, no. 1, p. 013115, Jan. 2017, doi: 10.1063/1.4974270.

[19] I. V. Bandurkin, V. L. Bratman, A. V. Savilov, S. V. Samsonov, and A. B. Volkov, "Experimental study of a fourth-harmonic gyromultiplier," *Phys. Plasmas*, vol. 16, no. 7, p. 070701, Jul. 2009, doi: 10.1063/1.3179805.

[20] R. C. Stutzman, D. B. McDermott, D. A. Gallagher, C. M. Armstrong, T. A. Spencer, and N. C. Luhmann, "Harmonic gyrotrons at 94 GHz," in *Proc. IEEE Int. Conf. Plasma Sci.*, Monterey, CA, 1999, p. 166, doi: 10.1109/PLASMA.1999.829424.

[21] M. Y. Glyavin, A. G. Luchinin, V. N. Manuilov, and G. S. Nusinovich, "Design of a subterahertz, third-harmonic, continuous-wave gyrotron," *IEEE Trans. Plasma Sci.*, vol. 36, no. 3, pp. 591-596, Jun. 2008, doi: 10.1109/TPS.2008.917530.

[22] X. Li, J. Lang, Y. Alfadhl, and X. Chen, "A high harmonic large orbit gyrotron in THz range," *Terahertz Sci. Technol.*, vol. 7, no. 4, pp. 181-187, Dec. 2014, doi: 10.11906/TST.181-187.2014.12.17.

[23] N. S. Ginzburg, M. Yu. Glyavin, A. M. Malkin, V. N. Manuilov, R. M. Rozental, A. S. Sedov, A. S. Sergeev,V. Yu. Zaslavsky, I. V. Zotova, and T. Idehara, "Improvement of stability of high cyclotron harmonic operation in the double-beam THz gyrotrons," *IEEE Trans. Plasma Sci.*, vol. 44, no. 8, pp. 1303–1309, Aug. 2016, doi: 10.1109/TPS.2016.2585307.

[24] I. V. Bandurkin, M. Yu. Glyavin, S. V. Kuzikov, P. B. Makhalov, I. V. Osharin, and A. V. Savilov, "Method of providing the high cyclotron harmonic operation selectivity in a gyrotron with a spatially developed operating mode," *IEEE Trans. Electron Devices*, vol. 64, no. 9, pp. 3893-3897, Sep. 2017, doi: 10.1109/TED.2017.2731982.

[25] Q. Zhao, S. Yu and T. Zhang, "Observation of mode competition in operation of a 420 GHz, $TE_{17,4}$ second harmonic gyrotron with complex cavity," *IEEE Trans. Electron Devices*, vol. 64, no. 11, pp. 4700-4705, Nov. 2017, doi: 10.1109/TED.2017.2756635

[26] V. I. Shcherbinin, V. I. Tkachenko, K. A. Avramidis, and J. Jelonnek, "Coaxial cavity with stepped inner conductor for a sub-terahertz second-harmonic gyrotron with broadband continuous frequency tuning," *IEEE Trans. Electron Devices*, vol. 66, no. 12, pp. 5313-5320, Dec. 2019, doi: 10.1109/TED.2019.2944647.

[27] V. I. Shcherbinin, "Multifunctional coaxial insert with distributed impedance corrugations for cavities of broadband tunable second-harmonic gyrotrons," *IEEE Trans. Electron Devices*, vol. 68, no. 8, pp. 4104-4109, Aug. 2021, doi: 10.1109/TED.2021.3090348.

[28] S. A. Malygin, "A high-power gyrotron operating at the third harmonic of the cyclotron frequency," *Sov. J. Commun. Technol. Electron.*, vol. 31, no. 6, pp. 106–108, June 1986.

[29] H. Li, Z.-L.Xie,W.Wang,Y. Luo, P.Du, X. Den, H. Wang, S.Yu, X. Niu, L. Wang, and S. Liu, "A 35-GHz low-voltage third-harmonic gyrotron with a permanent magnet system," *IEEE Trans. Plasma Sci.*, vol. 31, no. 2, pp. 264-271, April 2003, doi: 10.1109/TPS.2003.810732.

[30] V. L. Bratman, Y. K. Kalynov, and V. N. Manuilov, “Large-orbit gyrotron operation in the terahertz frequency range,” *Phys. Rev. Lett.*, vol. 102, no. 24, p. 245101, Jun. 2009, doi: 10.1103/PhysRevLett.102.245101.

[31] I. Bandurkin, A. Fedotov, M. Glyavin, T. Idehara, A. Malkin, V. Manuilov, A. Sergeev, A. Tsvetkov, V. Zaslavsky, and I. Zotova, "Development of third-harmonic 1.2-THz gyrotron with intentionally increased velocity spread of electrons," *IEEE Trans. Electron Devices*, vol. 67, no. 10, pp. 4432-4436, Oct. 2020, doi: 10.1109/TED.2020.3012524.

[32] V. I. Shcherbinin, K. A. Avramidis, I. Gr. Pagonakis, M. Thumm, and J. Jelonnek, "Large power increase enabled by high-Q diamond-loaded cavities for terahertz gyrotrons," *J. Infrared Millim. Terahertz Waves*, 2021, 10.1007/s10762-021-00814-6.

[33] V. I. Shcherbinin, K. A. Avramidis, M. Thumm and J. Jelonnek, "Mode discrimination by lossy dielectric rods in cavities of second-harmonic gyrotrons," *J. Infrared Millim. Terahertz Waves*, vol.42, no. 1, pp. 93-105, Jan. 2021, doi: 10.1007/s10762-020-00760-9.

[34] V. I. Shcherbinin, G. I. Zaginaylov, and V. I. Tkachenko, "HE and EH hybrid waves in a circular dielectric waveguide with an anisotropic impedance surface," *Problems Atomic Sci. Technol.*, no. 4 (98), pp. 89–93, Sep. 2015.

[35] V. I. Shcherbinin, G. I. Zaginaylov, and V. I. Tkachenko, "Analogy between circular core-cladding and impedance waveguides and their membrane functions," *Prog. Electromagn. Res. M*, vol. 53, pp. 111–120, 2017, doi: 10.2528/PIERM16110902.

[36] M. Thumm, "Development of output windows for high-power long-pulse gyrotrons and EC wave applications," *Int. J. Infrared Millim. Waves*, vol. 19, no. 1, pp 3–14, Jan. 1998, doi: 10.1023/A:1022514528711.

[37] R. Heidinger, G. Dammertz, A. Meier and M. K. Thumm, "CVD diamond windows studied with low- and high-power millimeter waves," *IEEE Trans. Plasma Sci.,* vol. 30, no. 3, pp. 800-807, June 2002, doi: 10.1109/TPS.2002.1158309.

[38] V. V. Parshin, M. Y. Tretyakov, M. A. Koshelev, and E. A. Serov, "Modern resonator spectroscopy at submillimeter wavelengths," *IEEE Sensors J.*, vol. 13, no. 1, pp. 18–23, Jan. 2013, doi: 10.1109/JSEN.2012.2215315.

[39] C.-H. Du and P.-K. Liu, “Nonlinear full-wave-interaction analysis of a gyrotron-traveling-wave-tube amplifier based on a lossy dielectric-lined circuit,” *Phys. Plasmas*, vol. 17, no. 3, p. 033104, Mar. 2010, doi: 10.1063/1.3339935.

[40] V. I. Shcherbinin, Y. K. Moskvitina, K. A. Avramidis and J. Jelonnek, "Improved mode selection in coaxial cavities for subterahertz second-harmonic gyrotrons," *IEEE Trans. Electron Devices*, vol. 67, no. 7, pp. 2933-2939, July 2020, doi: 10.1109/TED.2020.2996179.

[41] V. I. Shcherbinin, and V. I. Tkachenko, “Cylindrical cavity with distributed longitudinal corrugations for second harmonic gyrotron,” *J. Infrared Millim. Terahertz Waves*, vol. 38, no. 7, pp. 838–852, Jul. 2017, doi: 10.1007/s10762-017-0386-x.

[42] S. N. Vlasov, G. M. Zhislin, I. M. Orlova, M. I. Petelin, and G. G. Rogacheva, “Irregular waveguides as open resonators,” *Radiophys. Quantum Electron.*, vol. 12, no. 8, pp. 972–978, Aug. 1969, doi: 10.1007/BF01031202.

[43] V. L. Bratman, M. A Moiseev, M. I. Petelin, and R. É. Érm, "Theory of gyrotrons with a nonfixed structure of the high-frequency field," *Radiophys. Quantum Electron.*, vol. 16, no. 4, pp. 474–480, Apr. 1973, doi: 10.1007/BF01030898.

[44] V. N. Manuilov, A. I. Tsvetkov, M. Y. Glyavin, S. Mitsudo, T. Idehara, and I. V. Zotova, “Universal electron gun design for a CW third harmonic gyrotron with an operating frequency over 1 THz,” *J. Infrared Millim. Terahertz Waves*, vol. 41, no. 9, pp. 1121–1130, Sep. 2020, doi: 10.1007/s10762-020-00702-5.